Computers and Concrete, *Vol. 20, No. 3 (2017) 291-295*
DOI: https://doi.org/10.12989/cac.2017.20.3.291

Numerical approach to fracture behavior of CFRP/concrete bonded interfaces

Hai X. Lin*, Jian Y. Lu and Bing Xu

College of Civil Engineering, Henan Polytechnic University, Jiaozuo City, Henan Province, 454000, People's Republic of China

(Received March 17, 2016, Revised April 24, 2017, Accepted April 27, 2017)

Abstract. Tests on the fracture behavior of CFRP-concrete composite bonded interfaces have been extensively carried out. In this study, a progressive damage model is employed to simulate the fracture behaviors. The crack nucleation, propagation and more other details can be captured by these models. The numerical results indicate the fracture patterns seem to depend on the relative magnitudes of the interface cohesive strength and concrete tensile strength. The fracture pattern transits from the predominated adhesive-concrete interface debonding to the dominated concrete cohesive cracking as the interface cohesive strength changes from lower than concrete tensile strength to higher than that. The numerical results have an agreement with the experimental results.

Keywords: fracture behavior; CFRP composite; concrete; damage

1. Introduction

Strips, plates and sheets made of fiber-reinforced-polymers (FRP) are widely employed to strengthen and upgrade the existing concrete structures. It is well known that FRP composites have advantages in term of light weight, high tensile strength, durability. In practice, those properties make it promising alternative for construction industry and rehabilitation of existing reinforced concrete (RC) structures (Hao *et al.* 2009, Oded 2008, Taljsten 1996, Li *et al.* 2008, Lee *et al.* 2017). Rehabilitation of these structures can be in the form of strengthening of structural members, repair of damaged structures, or retrofitting for seismic deficiencies. In any case, composite materials are an excellent option to be used as external reinforcement. But the structural advantages require the FRP and the concrete bond well to ensure they work together. Much research work indicates that debonding along the FRP-concrete interface can lead to premature failure of the structure. Failure analysis of FRP-concrete bonded interfaces has steadily gained attention (Qian and Stroeve 2000, Kim and Pilakoutas 2009, Yehia 2009).

Fracture characterization of concrete and rock materials using the 3PBB specimens has been conducted extensively by researchers, such as Palmer and Baker (1991), Yon *et al*. (1991) and Shinohara *et al*. (2004). The preliminary application of the test method using notched three-point bending beam (3PBB) specimens for characterization of the fracture behaviors of carbon fiber-reinforced-polymers (CFRP)-concrete bonded interfaces was introduced by Qiao et al.(2004) and the CZM (cohesive zone model) (Chang *et al.* 2015a, 2015b, Chang *et al.* 2014) is adopted for the adhesive layer.

*Corresponding author, Ph.D.
E-mail: xulihuawhu@126.com

Although the aforementioned research work of fracture behaviors has been widely accepted, only few of the existing models can adequately reproduce the ongoing process of fracture nucleation, propagation, as observed experimentally. In addition, the analytical and numerical models considered so far tend to oversimplify the materials as a homogeneous medium. In our fracture modeling approach, more details of the fracture process can be captured.

2. Numerical approach

In the numerical model, the concrete material is assumed to be composed of many elements with the same size, and the mechanical properties of these elements are assumed to conform to a given Weibull distribution as defined in the following function

$$f(u)=\frac{m}{u_0}\left(\frac{u}{u_0}\right)^{m-1}\exp\left[-\left(\frac{u}{u_0}\right)^m\right] \quad (1)$$

where u is the parameter of the element (such as strength or elastic modulus); the scale parameter, u_0, is related to the average of the element parameter and the shape. Parameter, m, defines the shape of the distribution function. According to the definition, a larger m implies a more homogeneous material. We therefore call this parameter (m) the homogeneity index. In general, we assumed that the Young's modulus and strength (compression and tension) of mesoscopic elements that are used to simulate a concrete specimen conform to two individual distributions with the same homogeneity index. The mesoscopic elements are assumed to be isotropic and homogeneous (as shown in Fig. 1).

At the beginning, the element is considered elastic, and its elastic properties can be defined by Young's modulus and Poisson's ratio. The stress-strain curve of an element is

ISSN: 1598-8198 (Print), 1598-818X (Online)

considered linear elastic until the given damage threshold is attained, and then is followed by softening. We choose the maximum tensile stress criterion and Mohr-Coulomb criterion respectively as the damage thresholds. In elastic damage mechanics, the elastic modulus of the element may degrade gradually as damage progresses. The elastic modulus of damaged material is defined as follows (Tang *et al.* 2008).

$$E = (1-\omega)E_0 \tag{2}$$

where represents the damage variable, E and E_0 are elastic moduli of the damaged and the undamaged material, respectively. Here the element as well as its damage is assumed isotropic and elastic, so the E and E_0 are all scalar.

When the mesoscopic element is under a uniaxial stress state (including uniaxial compression and uniaxial tension), the constitutive relationship of elements is shown in Fig. 1. At the beginning, the stress-strain curve is linear elastic and no damage occurs, that is. The constitutive relationship of a mesoscopic element under uniaxial tension as shown in the third quadrant of Fig. 1 can be expressed as

$$\omega = \begin{cases} 0 & \varepsilon > \varepsilon_{t0} \\ 1-\dfrac{f_{tr}}{E_0\varepsilon} & \varepsilon_{tu} < \varepsilon \le \varepsilon_{t0} \\ 1 & \varepsilon \le \varepsilon_{tu} \end{cases} \tag{2}$$

where f_{tr} is the residual tensile strength defined as $f_{tr}=\lambda f_{t0}=\lambda E_0\varepsilon_{t0}$ and λ are uniaxial tensile strength and residual strength coefficients, respectively; ε_{t0} is the strain at the elastic limit (also called threshold strain); and ε_{tu} is the ultimate tensile strain of the element, at which the element would be completely damaged. The ultimate tensile strain is defined as $\varepsilon_{tu}=\eta\varepsilon_{t0}$, where η is called ultimate strain coefficient. Eq. (3) can be expressed as

$$\omega = \begin{cases} 0 & \varepsilon > \varepsilon_{t0} \\ 1-\dfrac{\lambda\varepsilon_{t0}}{\varepsilon} & \varepsilon_{tu} < \varepsilon \le \varepsilon_{t0} \\ 1 & \varepsilon \le \varepsilon_{tu} \end{cases} \tag{3}$$

Additionally, we assume that the damage of a mesoscopic element in a multiaxial stress condition is also isotropic and elastic. According to the method of extending a one-dimensional constitutive law under uniaxial tension to a complex stress condition, we can easily extend the constitutive law described above to use for three-dimensional stress states when the tensile strain threshold is attained. Under multi-axial stress states the element still damages in tensile mode when the equivalent major tensile strain $\bar{\varepsilon}$ attains the above threshold strain ε_{t0}. The equivalent principal strain $\bar{\varepsilon}_{t0}$ is defined as follows

$$\bar{\varepsilon}_{t0} = -\sqrt{\langle -\varepsilon_1\rangle^2 + \langle -\varepsilon_2\rangle^2 + \langle -\varepsilon_3\rangle^2} \tag{5}$$

where ε_1, ε_2 and ε_3 are three principal strains, and < >is a function defined as follows

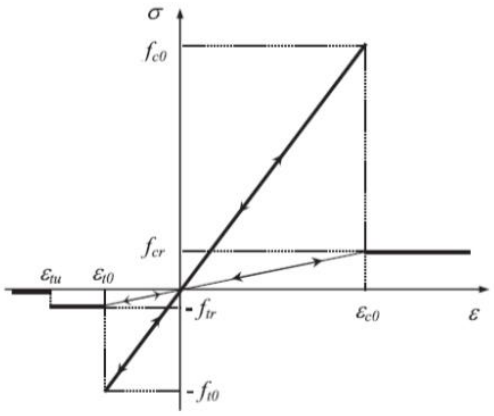

Fig. 1 Elastic damage constitutive law of elements under a uniaxial stress state

$$\langle x\rangle = \begin{cases} x & x \ge 0 \\ 0 & x < 0 \end{cases} \tag{6}$$

The constitutive law of the element subjected to multiaxial stresses can be easily obtained only by substituting the strain, ε, in Eqs. (3) and (4) with the equivalent strain, $\bar{\varepsilon}$. The damage variable is expressed as

$$\omega = \begin{cases} 0 & \bar{\varepsilon} > \varepsilon_{t0} \\ 1-\dfrac{\lambda\varepsilon_{t0}}{\bar{\varepsilon}} & \varepsilon_{tu} < \bar{\varepsilon} \le \varepsilon_{t0} \\ 1 & \bar{\varepsilon} \le \varepsilon_{tu} \end{cases} \tag{7}$$

In order to study the damage of an element when it is under compressive and shear stresses, the Mohr-Coulomb criterion is chosen to be the second damage threshold.

$$F = \sigma_1 = \frac{1+\sin\varphi}{1-\sin\varphi}\sigma_3 \ge f_{c0} \tag{8}$$

where σ_1 and σ_2 are major and minor principal stress respectively; f_{c0} is the uniaxial compressive strength and is the internal friction angle of the mesoscopic element. Again, compressive stresses are positive and tensile stresses are negative. As a matter of fact, the numerical values of σ_1 and σ_3 indicate the magnitude of maximum and minimum compressive stresses, respectively, when these two principal stresses are both compressive. In the same way, when the element is under uniaxial compression and damage according to the Mohr-Coulomb criterion, the similar expression for the damage variable, ω, can be described as follows

$$\omega = \begin{cases} 0 & \varepsilon < \varepsilon_{c0} \\ 1-\dfrac{\zeta\varepsilon_{c0}}{\varepsilon} & \varepsilon \ge \varepsilon_{c0} \end{cases} \tag{9}$$

where ζ is the residual strength coefficient. We assumed that $f_{cr}/f_{c0}=f_{tr}/f_{t0}=\zeta$ is true when element is under uniaxial compression or tension; f_{cr} is the residual compressive

strength.

When an element is under a multi-axial stress state and its strength satisfies the Mohr-Coulomb criterion, damage occurs, and we must consider the effect of other principal stresses in this model during the damage evolution process. When the Mohr-Coulomb criterion is met, we can calculate the maximum principal strain (maximum compressive principal strain) ε_{c0} at the peak value of maximum principal stress (maximum compressive principal stress).

$$\varepsilon_{c0} = \frac{1}{E_0}\left[f_{c0} + \frac{1+\sin\varphi}{1-\sin\varphi}\sigma_3 - u\left(\sigma_1+\sigma_2\right)\right] \quad (10)$$

where σ_2 is the intermediate principal stress.

In this respect, we assume that the shear damage evolution is only related to the maximum compressive principal strain, ε_1. So, we use the maximum compressive principal strain, ε_1, of the damaged element to substitute the uniaxial compressive strain, ε in Eq. (9). Thus, the former Eq. (9) can be extended to triaxial stress states for shear damage.

$$\omega = \begin{cases} 0 & \varepsilon_1 < \varepsilon_{c0} \\ 1-\dfrac{\zeta\varepsilon_{c0}}{\varepsilon_1} & \varepsilon_1 \geq \varepsilon_{c0} \end{cases} \quad (11)$$

In summary, our numerical approach to the fracture problem can be described as the following: Our numerical simulation involves the calculation of the stresses acting on the elements and the mechanical property change of the damaged elements according to the constitutive laws and strength criterion described above. The value at which a particular element fails is random, but fixed at the start of the modeling process. The statistical distribution of the breakdown thresholds is a material property and is described by Eq. (1). Under a quasi-statically increasing external stretch the stress or strain of the elements are given by the solution of the FEM for mechanical equilibrium at each FEM node. If the stress of an element attains its prescribed breakdown strength, the element fails irreversibly, and its elastic constant is changed according to its post-failure law, as described above. This is followed by additional relaxation steps, in which the new equilibrium positions are calculated. In the brittle regime these steps may lead to the failure of additional elements. Iterating the procedure leads to fracture propagation, where fractures are defined by groups and alignments of failed elements (Tang *et al*. 2008).

3. Finite element model

The aforementioned damage models are implemented in finite element (FE) modeling of the 3PBB beam specimens containing CFRP-concrete bonded interfaces. The four-node isoparametric element is used as the basic element in the finite element mesh and a single layer of 2-D cohesive elements through the thickness of adhesive for the cohesive zone is adopted to model the bond behavior. The model is numerically simulated as plane stress problem. The model, its boundary and loading conditions and the FEM mesh are shown in Fig. 2. The model has a length of 900 mm and thickness of 100 and contains a total of about 90,000 elements, each 1 mm square for concrete and CFRP composite materials. To accurately capture the interface failure process, the small element size for the cohesive layer is 0.5 mm. Loading of the 3PBB specimen with CFRP-concrete bonded interface is applied symmetrically through imposed displacement at the center of the beam on the top edge, the same as in the experiment.

As real materials, CFRP-concrete composite structures are never homogeneous medium because they contain inhomogeneities, such as imperfection of CFRP-concrete bond and defects at various length-scales in concrete subrate. It is necessary to consider these local-scale heterogeneities in fracture modeling. In our numerical

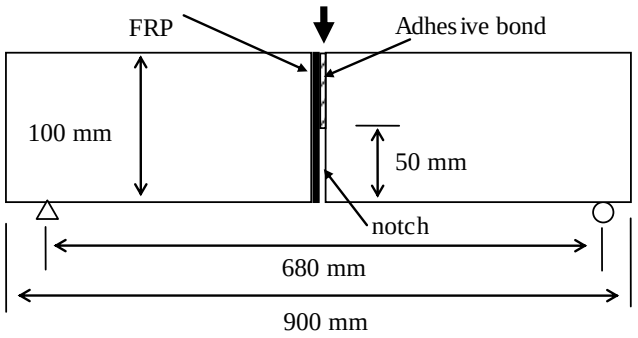

Fig. 2 Sketch of composite-concrete bonded interface 3PBB specimen

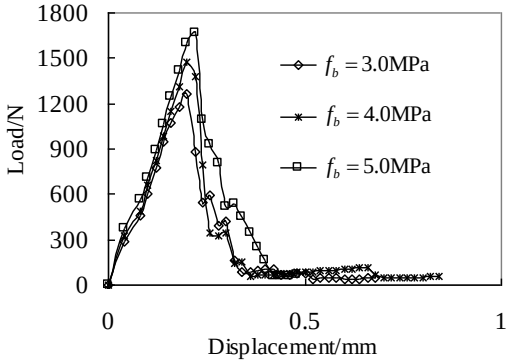

Fig. 3 Load-displacement curve with a given concrete tensile f_t=6.0 MPa

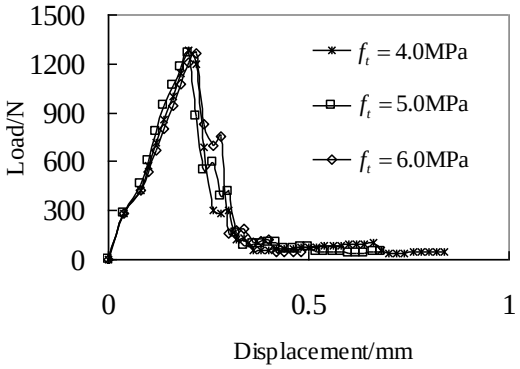

Fig. 4 Load-displacement curve with a given interface cohesive strength of f_b=3.0 MPa

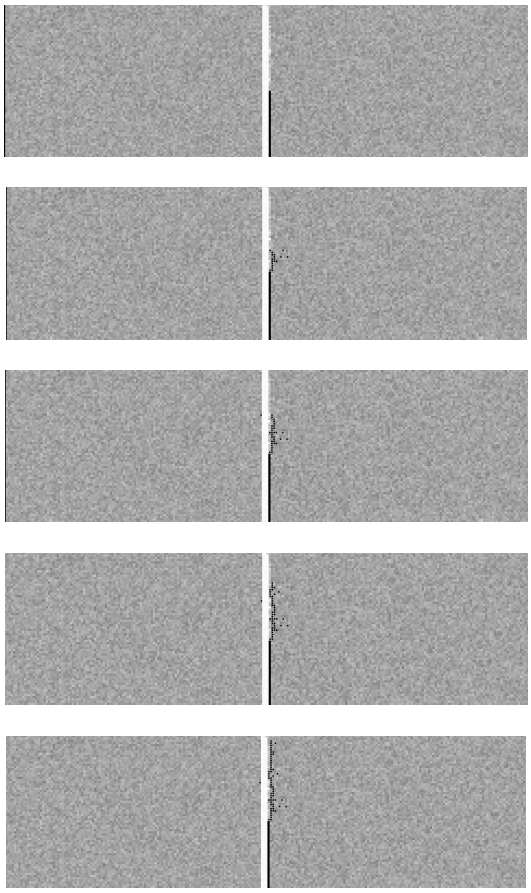

Fig. 6 The co-existence fracture propagation process of adhesive concrete interface debonding and concrete cohesive cracking when the interface cohesive strength is comparative to the concrete tensile strength

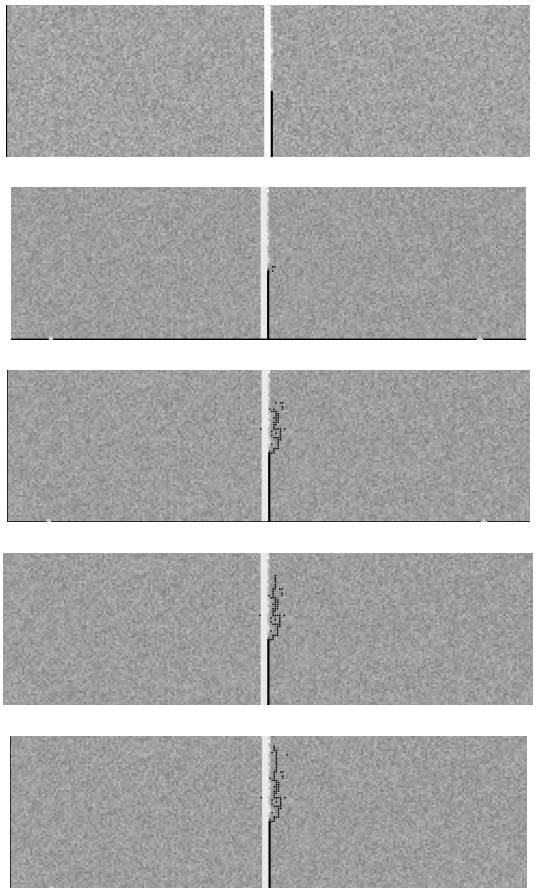

Fig. 7 The fracture propagates in the concrete substrate along the interface when the interface cohesive strength is kept higher than the concrete tensile strength

study, this is accommodated by the implicit inclusion of heterogeneity through the homogeneity index, *m*, is described in Eq. (1). The FEM model we used comprises a large number of elements, and its local heterogeneity is determined by assigning to each element a group of mechanical parameters, such as Young's modulus, strength, et cetera, from the given statistical distribution Eq. (1). The extent of the heterogeneity is represented by an index of *m*=3. The constitutive relationship for composite materials is shown in Fig. 1 and the elastic modulus for the concrete is 34 GPa.

According to investigation by Qiao and Chen (2008), the normal cohesive strength of the CFRP-concrete interface ranging from 3.0 to 7.0 MPa is considered in this study and the concrete tensile strength varies from 3.0 to 7.0 MPa. The elastic modulus of CFRP is 227 GPa.

4. Numerical results

The interface cohesive strength and the concrete tensile strength are two important factors controlling the interface fracture behavior. As an attempt to investigate effects of interface cohesive strength in relationship with the concrete tensile strength on fracture behaviors, the fracture process and load-displacement curve are simulated by the numerical model mentioned above. The load-displacement curves are compared in Fig. 3 and Fig. 4. In Fig. 3, the interface cohesive strength (f_b) ranges from 3.0 to 5.0 MPa with a given concrete tensile strength of 6.0. In Fig. 4, the interface cohesive strength is 3.0 MPa and the concrete tensile strength (f_t) increases from 4.0 to 6.0 MPa. Obviously, the peak loads seem to depend on the interface cohesive strength when the interface cohesive strength is kept lower than the concrete tensile strength. The lower the interface cohesive strength, the lower the peak loads. However, there is no apparent difference of loads with increasing concrete tensile strength. In this case, the crack initiates at the pre-existed notch and propagates to the load point along the interface with increasing external load, as shown in Fig. 5. Obviously, the fracture is primarily dominated by the interface cohesive failure. The numerical results have a good agreement with the test results (Qiao and Chen 2008).

When the interface cohesive strength is comparative to the concrete tensile strength, the interface failure is controlled by the co-existence of adhesive-concrete interface debonding and concrete cohesive cracking (Chang *et al.* 2014), as shown in Fig 6. We note that failure phenomena depend very strongly on the properties of the material disorder and thus the involved materials cannot be treated as a homogeneous medium. Fracture of heterogeneous solids typically initiates from scattered weak sites. In our model, the mechanical properties of the

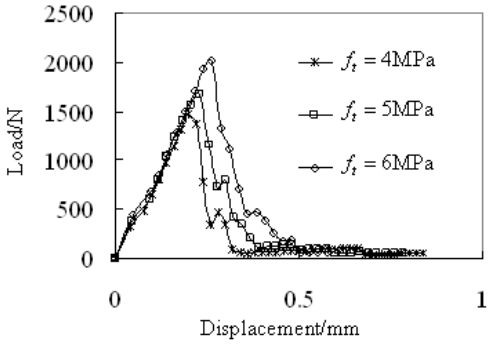

Fig. 8 Load-displacement curve with a given interface cohesive strength of f_b=7.0 MPa

elements are assumed to conform the Weibell distribution and the failure elements are randomly distributed, so the fracture alternately propagates at the interface cohesive or concrete substrate when they have the approximating strength.

When the interface cohesive strength is higher than concrete tensile strength, the interface failure is fully controlled by the concrete cohesive cracking along the interface line, as shown in Fig. 7. The fracture propagates from the notch to the load point in the concrete substrate along the interface. In this case, the peak loads seem to depend on the concrete tensile strength. Higher the concrete tensile strength leads to higher the peak load (see Fig. 8). However, no obvious difference of peak load can be observed with increasing the interface cohesive strength.

5. Conclusions

In this paper we performed numerical studies of fracture behavior of the CFRP-concrete bonded interfaces in the 3PBB configuration. The numerical simulation can adequately reproduce the ongoing process of fracture nucleation and propagation, which has a good agreement with test results.

The fracture pattern seems to depend on the relationship between the interface cohesive strength and the concrete tensile strength. Imperfection of CFRP–concrete bond with a low interface cohesive strength (especially when the interface cohesive strength is relatively lower than the concrete tensile strength) cause the premature interface cohesive failure, thus greatly reducing the CFRP strengthening performance. When the interface cohesive strength is higher than the concrete tensile strength, the interface failure mainly propagates through the concrete cohesive cracking along the bond line. In this case, the peak load mainly depends on the concrete tensile strength.

Acknowledgments

The research reported in this paper is supported by the Key Subject Foundation of Henan Province (No 504906. The financial support is highly appreciated.

References

Chang, X., Luo, X.L., Zhu, C.X. and Tang, C.A. (2014), "Analysis of circular concrete-filled steel tube support in high ground stress conditions", *Tunn. Undergr. Sp. Technol*., 41-48.

Chang, X. Shan, Y.F., Zhang, Z.H., Tang, C.A. and Ru, Z.L. (2015b), "Behavior of propagating fracture at bedding interface in layered rocks", *Eng. Geo*., **41**, 33-41.

Chang, X., Wang, J.H., Zhang, Z.H. and Tang, C.A. (2015a), "Effects of interface behavior on fracture spacing in layered rock", *Rock Mech. Rock Eng*., **49**(5), 1733-1746.

Hao, Q., Wang, Y., He, Z. and Ou, J. (2009), "Bond strength of glass fiber reinforced polymer ribbed rebars in normal strength concrete", *Constr. Build. Mater*., **23**(2), 865-871.

Kim, G.B. and Pilakoutas, K.P. (2009), "Waldron. Finite element analysis of thin GFRC panels reinforced with FRP", *Constr. Build. Mater*., **23**(2), 930-942

Lee, D.H., Han, S.J., Kim, K.S. and LaFave, J.M. (2017), "Shear strength of reinforced concrete beams strengthened in shear using externally-bonded FRP composites", *Compos. Struct*., **173**, 177-187.

Li, L., Guo, Y. and Liu, F. (2008), "Test analysis for FRC beams strengthened with externally bonded FRP sheets", *Constr. Build. Mater*., **22**(3), 315-323.

Oded, R. (2008), "Debonding analysis of fiber-reinforced-polymer strengthened beams: Cohesivezone modeling versus a linear elastic fracture mechanics approach", *Eng. Fract. Mech*., **75**(10), 2842-2859.

Palmer, G.B. and Baker, G. (1991), "Fracture toughness and size effect in low-cement refractories", *Fract. Proc. Concrete Rock Ceram*., **1**, 387-396.

Qian, C. and Stroeven, P. (2000), "Fracture properties of concrete reinforced with steel-polypropylene hybrid fibres", *Cement Concrete Compos*., **22**(5), 343-351.

Qiao, P. and Chen, Z.Y. (2008), "Cohesive fracture simulation and failure modes of FRP-concrete bonded interfaces", *Theor. Appl. Fract. Mech*., **49**(2), 213-225.

Qiao, P. and Xu, Y.W. (2004), "Evaluation of fracture energy of composite bonded interfaces usingthree-point bend tests", *J. Compos. Constr*., **8**(4), 352-359.

Taljsten, B. (1996), "Strengthening of concrete prism using the plate-bonding technique", *J. Fract*., **82**(3), 253-266.

Tang, C.A., Liang, Z.Z., Zhang, Y.B. and Chang, X. (2008), "Fracture spacing in layered materials: A new explanation based on two-dimensional failure process modeling", *Am. J. Sci*., **308**(1), 49-72.

Yehia, N.A.B. (2009), "Fracture mechanics approach for flexural strengthening of reinforced concrete beams", *Eng. Str*., **31**(2), 404-416.

CC